

Yttrium Doping of Perovskite Oxide $\text{La}_2\text{Ti}_2\text{O}_7$ Nanosheets for Enhanced Proton Conduction and Gas Sensing Under High Humidity Levels

Jian Wang, Caicai Sun, Jusheng Bao, Zhiwei Yang, Jian Zhang* and Xiao Huang*

Institute of Advanced Materials (IAM), School of Flexible Electronics (SoFE), Nanjing Tech University (NanjingTech), 30 South Puzhu Road, Nanjing 211816, China; 202262122006@njtech.edu.cn (J.W.); suncaicai202261122082@njtech.edu.cn (C.S.); baojsh@ahstu.edu.cn (J.B.); 202362221243@njtech.edu.cn (Z.Y.)
 * Correspondence: iamjzhang@njtech.edu.cn (J.Z.); iamxhuang@njtech.edu.cn (X.H.)

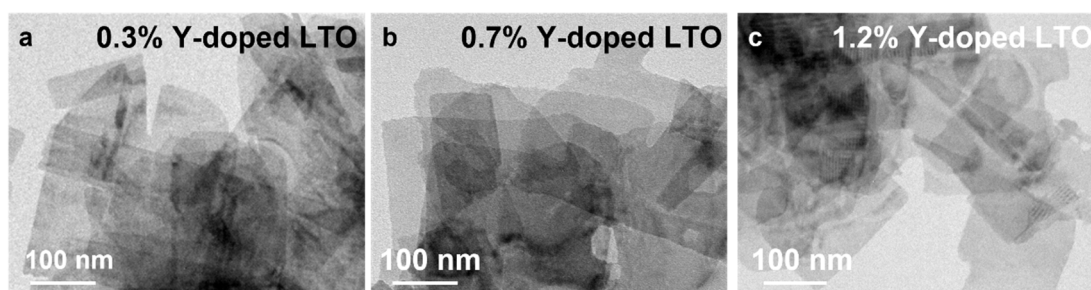


Figure S1. TEM images of (a) 0.3%, (b) 0.7% and (c) 1.2% Y-doped LTO nanosheets.

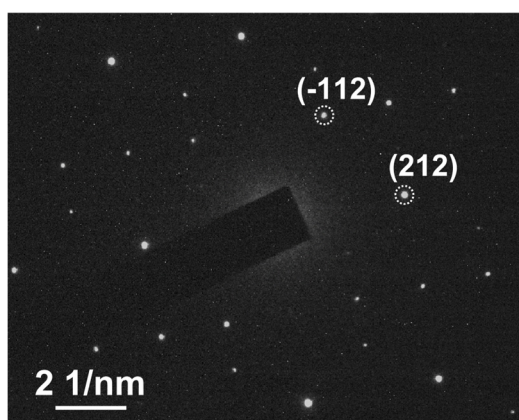


Figure S2. SAED pattern of 0.7% Y-doped LTO nanosheet.

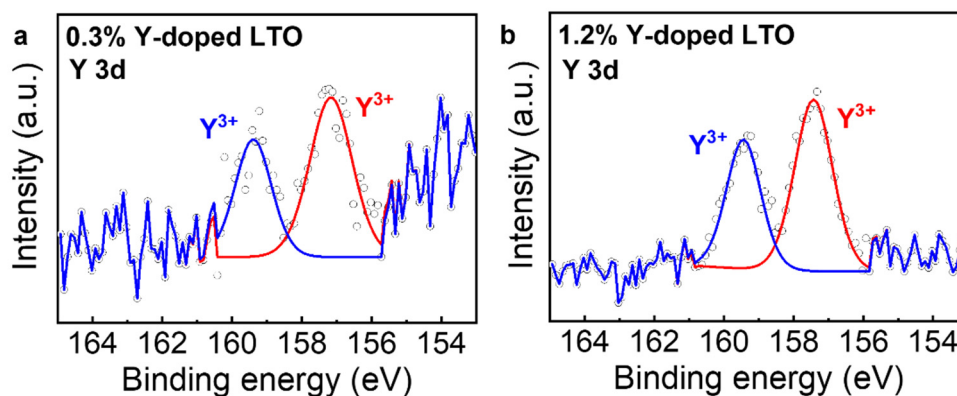


Figure S3. High-resolution Y 3d spectra of (a) 0.3% and (b) 1.2% Y-doped LTO nanosheets.

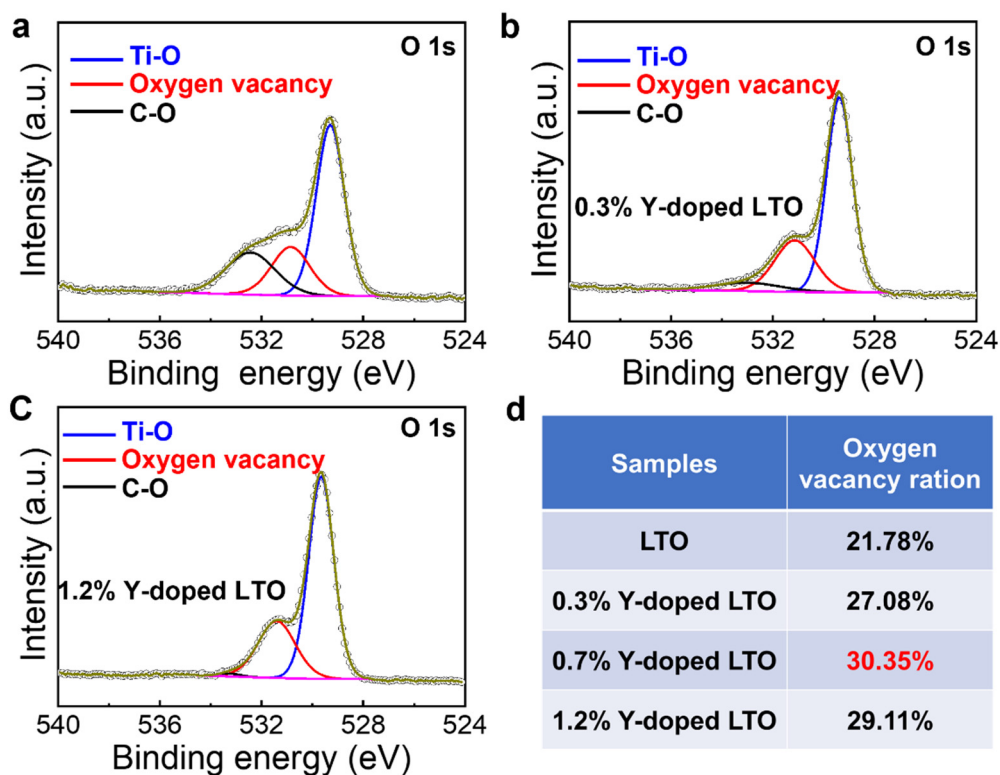


Figure S4. High-resolution O 1s spectra of (a) pure LTO, (b) 0.3% and (c) 1.2% Y-doped LTO nanosheets. (d) Oxygen vacancy ratio table of YLTO nanosheets.

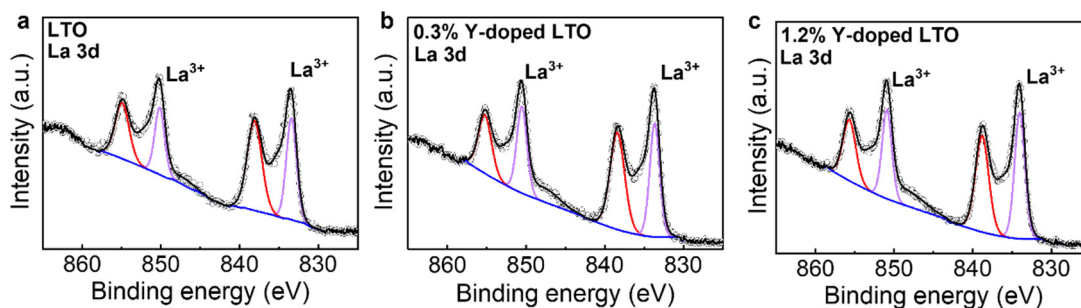


Figure S5. High-resolution La 3d spectra of (a) pure LTO, (b) 0.3% and (c) 1.2% Y-doped LTO nanosheets.

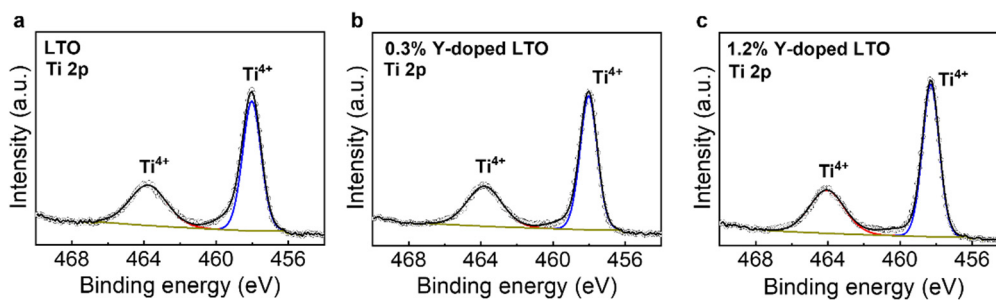


Figure S6. High-resolution Ti 2p spectra of (a) pure LTO, (b) 0.3% and (c) 1.2% Y-doped LTO nanosheets.

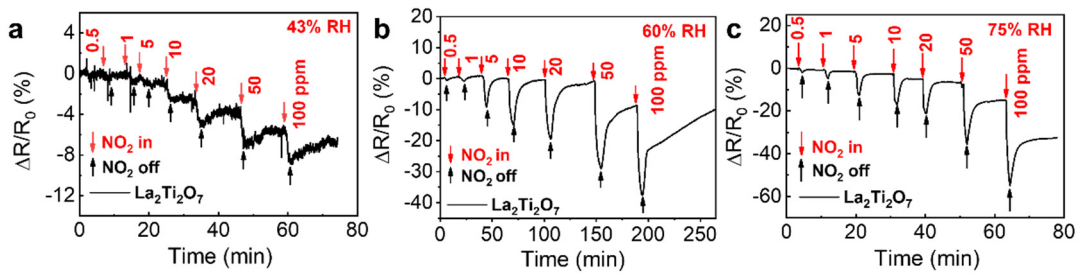


Figure S7. Sensing responses of LTO nanosheets to NO₂ under (a) 43% RH, (b) 60% RH and (c) 75% RH.

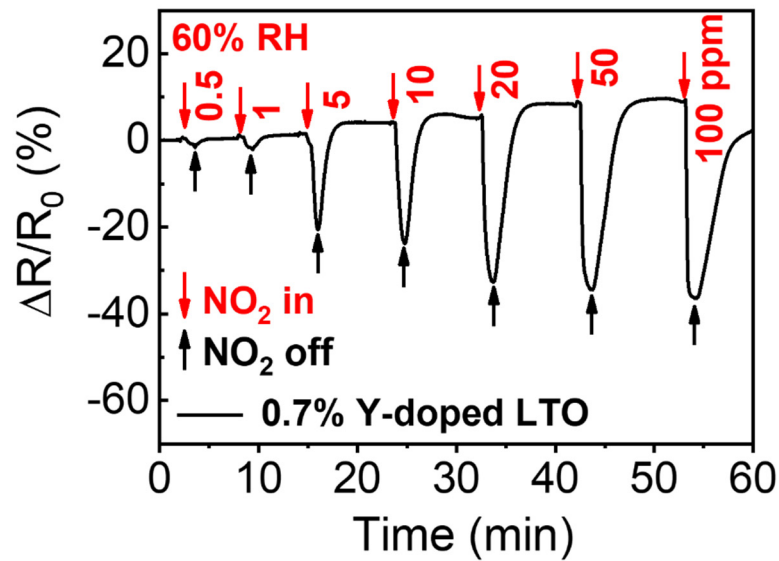


Figure S8. Sensing responses of 0.7% Y-doped LTO nanosheets to NO₂ under 60% RH.

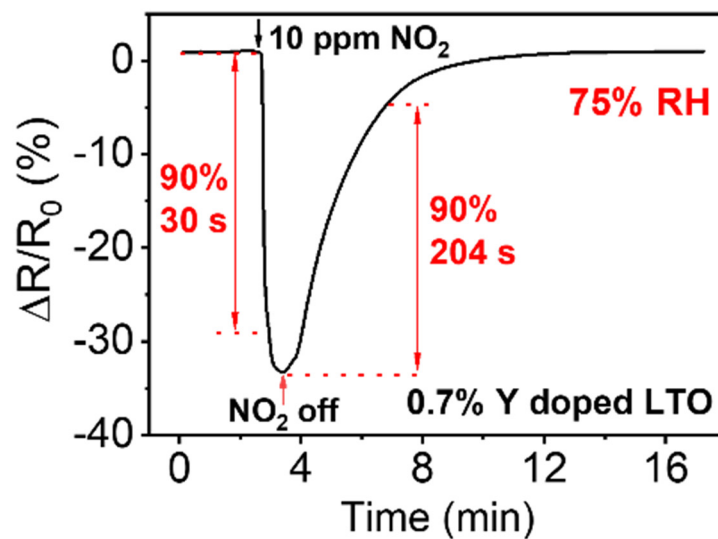


Figure S9. Dynamic response-recovery curves of 0.7% Y doped LTO to 10 ppm NO₂ at 75% RH.

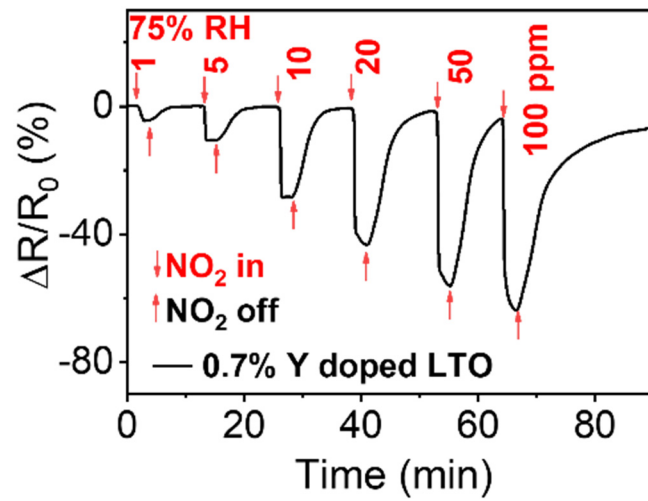


Figure S10. Dynamic response-recovery curves of 0.7% Y doped LTO after one week standing.

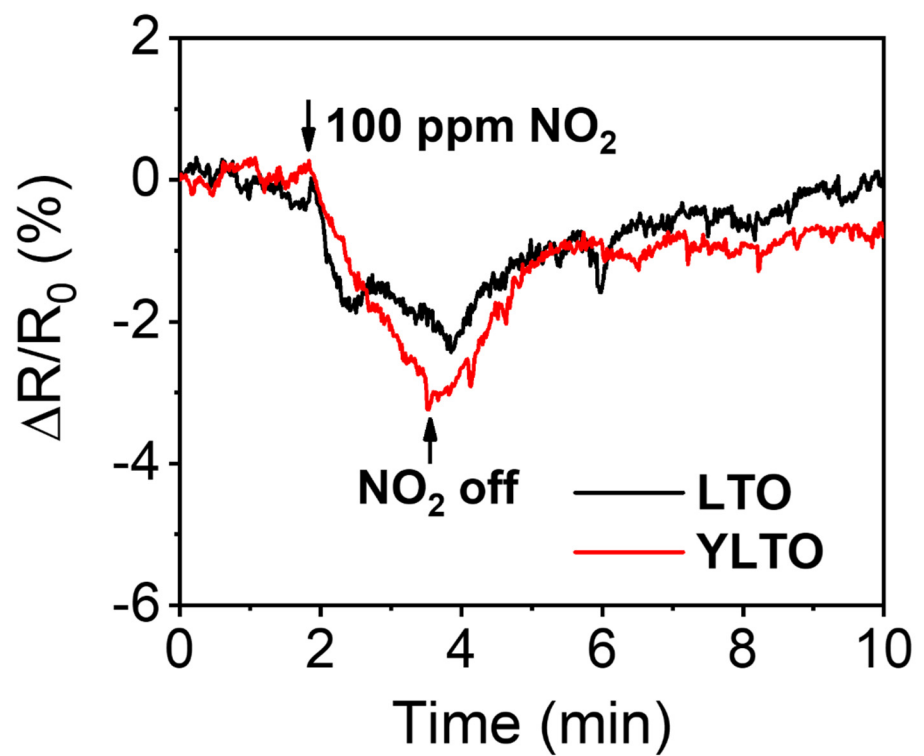


Figure S11. Sensing responses of LTO and 0.7% Y-doped LTO nanosheets to 100 ppm NO₂ under 23 % RH.

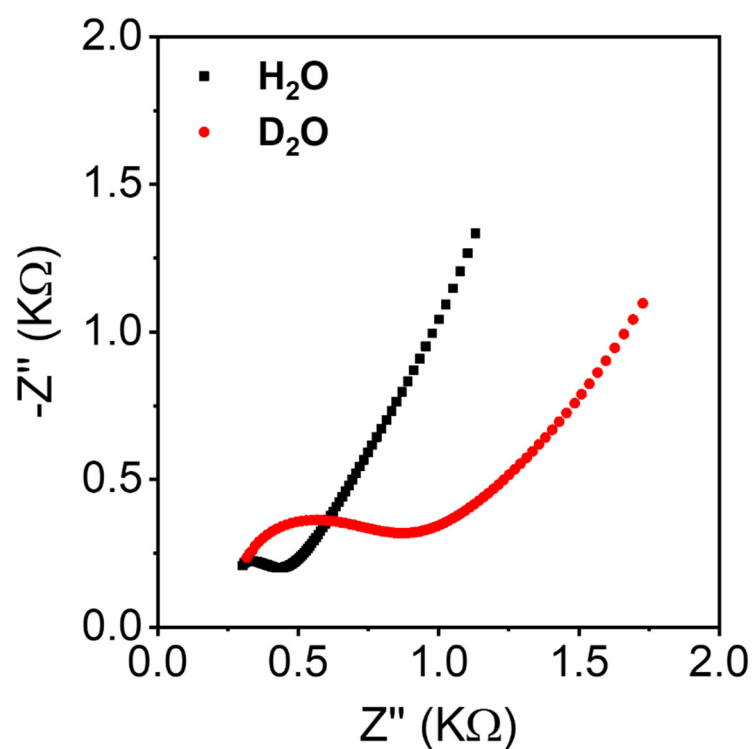


Figure S12. Nyquist plot of LTO nanosheet in H₂O and D₂O environments under 100% RH.

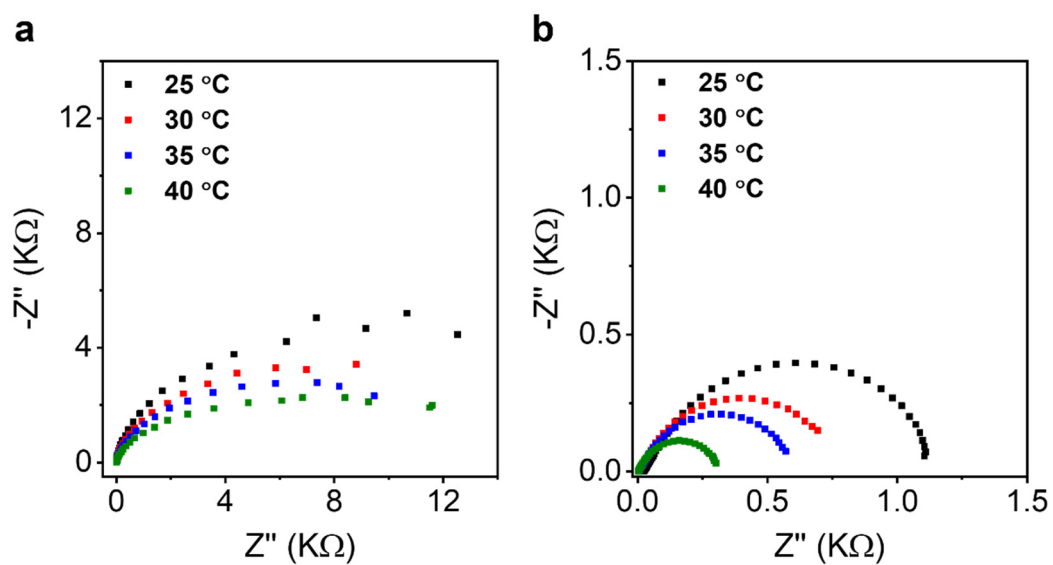


Figure S13. Nyquist plots of 0.7% Y-doped LTO nanosheets under (a) 43% RH and (b) 75% RH.

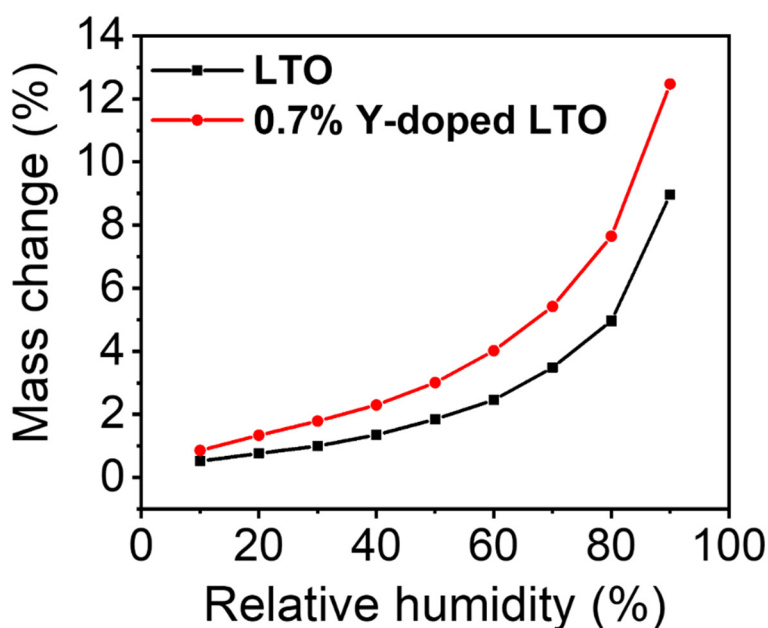


Figure S14. Water adsorption curves of LTO and 0.7% Y-doped LTO nanosheets.

Table S1. Comparison of the sensing performance of the recently reported NO₂ sensors based single-component metal oxides.

Material	Humidity Tolerance	Response	Response/Recovery Time	Detection Limit (ppm)	Ref.
YLTO	43% -75% RH	36% @ 10 ppm	30 s/204 s @ 10 ppm	0.5	This work
CuO	30% - 70% RH	33.3% @ 20 ppm	8 s/176 s @ 10 ppm	1	[1]
Ce ₂ Sn ₂ O ₇	70% - 85% RH	53% @ 50 ppm	4 s/52 s @ 10 ppm	0.5	[2]
WO ₃	Decreased response under high RH	45% @ 50 ppm, 250 °C	75 s/33 s @ 50 ppm	1	[3]
WO ₃	Unstable response under high RH	20% @ 3 ppm	50 s/300 s @ 3 ppm	3	[4]
In ₂ O ₃	~ 40% RH	35% @ 5 ppm, 400 °C	5 min/30 min @ 5 ppm	0.2	[5]
ZnO	Decreased response under high RH	43.7% @ 10 ppm, 300 °C	80 s/65 s @ 10 ppm	2	[6]
ZnO	/	36.4% @ 100 ppm, 200 °C	25 s/320 s @ 100 ppm	4	[7]

References:

- Chen, X.; Zhao, S.; Zhou, P.; Cui, B.; Liu, W.; Wei, D.; Shen, Y. Room-temperature NO₂ sensing properties and mechanism of CuO nanorods with Au functionalization. *Sens. Actuators, B* **2021**, *328*, 129070, doi:10.1016/j.snb.2020.129070.
- Ganesan, M.; Jayaraman, V.; Selvaraj, P.; Mani, K.M.; Kim, D.-H. Pyrochlore cerium stannate (Ce₂Sn₂O₇) for highly sensitive NO₂ gas sensing at room temperature. *Appl. Surf. Sci.* **2023**, *624*, 157135, doi:10.1016/j.apusc.2023.157135.
- Dwivedi, C.; Srivastava, S.; Singh, P. Highly selective dual gas (NO & NO₂) sensing depended on the operating temperature of WO₃ thin films sputtered at room temperature. *Curr. Appl. Phys.* **2025**, *69*, 70-80, doi:10.1016/j.cap.2024.11.009.
- Ghosh, S.; Ilango, M.S.; Prajapati, C.S.; Bhat, N. Reduction of Humidity Effect in WO₃ Thin Film-Based NO₂

- Sensor Using Physiochemical Optimization. *Cryst. Res. Technol.* **2020**, *56*, 2000155, doi:10.1002/crat.202000155.
5. D'Olimpio, G.; Boukhvalov, D.W.; Galstyan, V.; Occhiuzzi, J.; Vorochta, M.; Amati, M.; Milosz, Z.; Gregoratti, L.; Istrate, M.C.; Kuo, C.-N.; et al. Unlocking superior NO₂ sensitivity and selectivity: the role of sulfur abstraction in indium sulfide (InS) nanosheet-based sensors. *J. Mater. Chem. A* **2024**, *12*, 10329-10340, doi:10.1039/D4TA01287A.
 6. Bang, J.H.; Kwon, Y.J.; Lee, J.H.; Mirzaei, A.; Lee, H.Y.; Choi, H.; Kim, S.S.; Jeong, Y.K.; Kim, H.W. Proton-beam engineered surface-point defects for highly sensitive and reliable NO₂ sensing under humid environments. *J. Hazard. Mater.* **2021**, *416*, 125841, doi:10.1016/j.jhazmat.2021.125841.
 7. Ambi, R.R.; Mulla, M.G.; Pittala, R.K. NO₂ sensing properties of chemically deposited vertically aligned flowerlike hexagonal ZnO nanorods. *Sens. Actuators, A* **2024**, *376*, 115621, doi:10.1016/j.sna.2024.115621.